Published in final edited form as:
Contrast Media Mol Imaging. 2015 January ; 10(1): 74–80. doi:10.1002/cmmi.1597.

Anthranilic acid analogues as diamagnetic CEST (diaCEST) MRI contrast agents that feature an IntraMolecular-bond Shifted HYdrogen (IM-SHY)

Xiaolei Song[a,b,#], **Xing Yang**[a,#], **Sangeeta Ray Banerjee**[a], **Martin G. Pomper**[a,*], and **Michael T. McMahon**[a,b,*]

[a]Russell H. Morgan Department of Radiology and Radiological Science The Johns Hopkins University School of Medicine, Baltimore, Maryland, USA.

[b]F.M. Kirby Research Center for Functional Brain Imaging, Kennedy Krieger Institute, Baltimore, Maryland, USA

Abstract

Diamagnetic chemical exchange saturation transfer (diaCEST) agents are a new class of imaging agents, which have unique magnetic resonance (MR) properties similar to agents used for optical imaging. Here we present a series of anthranilic acid analogues as examples of diaCEST agents that feature an exchangeable proton shifted downfield, namely, a IntraMolecular-bond Shifted Hydrogen (IM-SHY), which produce significant and tunable contrast at frequencies of 4.8 – 9.3 ppm from water. Five analogues of N-sulfonyl anthranilic acids are all highly soluble and produced similar CEST contrast at ~ 6 – 8 ppm. We also discovered that flufenamic acid, a commercial non-steroidal anti-inflammatory drug, displayed CEST contrast at 4.8 ppm. For these N-H IM-SHY agents, the contrast produced was insensitive to pH making these complementary to existing diaCEST probes. This initial IM-SHY library includes the largest reported shifts for N-H protons on small organic diaCEST agents, and should find use as multi-frequency MR agents for *in vivo* applications.

Keywords

chemical exchange saturation transfer; N-sulfonyl anthranilic acid derivatives; molecular imaging; N-aryl anthranilic acid derivatives

Introduction

Chemical exchange saturation transfer (CEST) contrast agents, first introduced in 2000(1), are an alternative to traditional magnetic resonance (MR) contrast agents, which rely on direct enhancement of water relaxivity. The CEST mechanism involves saturation of labile

[*]Corresponding author(s): Michael T. McMahon, Phone: +1-443-923-9356, Fax: 1-443-923-9505, mcmahon@mri.jhu.edu, Address: F.M. Kirby Research Center for Functional Brain Imaging, Kennedy Krieger Institute, 707 N. Broadway, Baltimore, MD 21287, Martin G. Pomper, Phone: +1-410-955-2789, Fax: 1-443-817-0990, mpomper@jhmi.edu, Address: CRB II, 1550 Orleans Street, Baltimore, MD, 21231.
[#]X.S. and X.Y. contributed equally to this work

protons on the agents *via* selectively-irradiation at their resonance frequencies. The signal loss is then transferred to surrounding bulk water through chemical exchange, leading to a reduction in water signal (2–4). This water signal loss (CEST contrast) results in an amplification of the signal from low-concentration protons through the multiple exchange events occurring during the saturation pulse. Because the CEST contrast is derived from irradiation at a specific proton frequency, it is easier to discriminate from other sources of signal change than T1 or T2* contrast. This frequency dependence of contrast also allows the simultaneous detection and discrimination of multiple agents within an image(5–7). Diamagnetic CEST (diaCEST) and paramagnetic CEST (paraCEST) agents have been the subjects of several recent reviews(8–11). DiaCEST agents, such as glucose(12–14), glycogen(15), myo-inositol(16), glutamate(17), creatine(18,19), L-arginine(20,21), glycosaminoglycans(22,23) and peptides(5,24–26) are attractive biocompatible materials, but compared with paraCEST agents(27), they suffer from reduced sensitivity due to the relatively small chemical shift difference between their exchangeable protons and those of water (1–5.0 ppm). To address this issue, diaCEST agents with protons of increased chemical shift have been reported, including the thymidine analogues (5.5 ppm)(28) and iopamidol (4.2 and 5.5 ppm)(29,30). Most recently, we reported that the C2-OH in 2-hydroxybenzoic acid analogues resonates between 8.7 – 10.8 ppm from water, with solute-to-water exchange rates (k_{sw}) that are well suitable for CEST imaging(31). Building upon that report, here we describe the anthranilic acid analogues: N-aryl derivatives, N-acyl derivatives and N-sulfonyl derivatives, as another class of IntraMolecular-bond Shifted Hydrogens exchangeable proton (IM-SHY) diaCEST agents, based on the exchange of N-H protons instead of O-H (Scheme 1).

Results and Discussion

Salicylic acid (**1**) displays CEST contrast at 9.3 ppm (31) (Fig. 1). This dramatic chemical shift derives from the low barrier hydrogen bond between the exchangeable phenolic proton and the carboxylate anion at neutral pH(32,33). We also determined that similar CEST signals could be observed in other compounds with the 2-hydroxybenzoic acid scaffold, representing a powerful new type of CEST agent, based on the principle of IM-SHY(31). We were interested in preparing similar agents with labile anthranilic rather than phenolic protons to explore further the capabilities of the benzoic acid core for generating CEST contrast. However, anthranilic acid (**2**), an N-H analogue of salicylic acid, failed to produce contrast (Scheme 1, Fig. 1). To understand why, we measured the CEST contrast properties of a wide range of common anthranilic acid analogues, including those with N-alkyl, N-aryl, N-acyl, and N-sulfonyl substitutions (Scheme 1). Interestingly, significant contrast was observed in N-phenylanthranilic acid (**4**), although the labile protons resonate at 4.8 ppm, which is much lower than the 9.3 ppm observed in **1**. At a relatively low saturation field strength (B_1) = 3.6 μT, **4** showed a broader peak in the CEST MTR_{asym} spectrum than that of **1** and **12** (Fig. 1b), indicating a faster exchange. Using the QUESP experiment (34) we measured k_{sw} = 2.0 kHz (supplemental Fig. S1), which is slightly too fast to obtain optimal CEST contrast using the 3 – 5 μT saturation pulses we are able to employ on our clinical scanners. Comparing the CEST signal between **4** and **2**, the loss of CEST signal in **2** indicates that k_{sw} is too high. This is possibly due to the presence of the additional non-

hydrogen-bonded C2 N-H proton, which might undergo a fast intramolecular exchange with the hydrogen-bonded proton. In addition, if we modify **2** through substitution of a methyl group for one of the amine protons (**3**), the CEST contrast is still absent, which implies stereoelectronic influences are also important (Scheme 1). It is worth mentioning that N-phenylanthranilic acid analogues are commonly used as non-steroidal anti-inflammatory drugs (NSAIDs). The CEST properties were measured on five commercially available drugs, including flufenamic acid (**5**), meclofenamic acid (**6**), mefenamic acid (**7**), tolfenamic acid (**8**) and niflumic acid (**9**). Their water solubility is generally low (~ 10 mM or lower). As shown in Scheme 1, flufenamic acid (**5**) showed similar CEST properties to **4**. The exchangeable proton resonates at 4.8 ppm, with k_{sw} = 1.0 kHz. The CEST data of **6, 7** and **8** indicated the importance of steric interaction on the proton exchange rate with water. Adding the chloro group ortho to the exchangeable N-H (**6**) reduced its water accessibility and the CEST contrast dropped to 1%. This is presumably because the exchange is too slow, however, it's difficult to quantify k_{sw} because of the small contrast. Increasing the steric hindrance through addition of methyl (**7** and **8**) eliminated the CEST signal. Niflumic acid (**9**), the pyridine analogue of **5**, did not display any CEST contrast. One possible explanation is that the presence of the pyridine nitrogen tends to strongly hydrogen bond to water and alters the proton exchange of the IM-SHY -NH.

We next determined the detection limits of **5** with CEST, because it could potentially be translated into clinical applications(35). The solubility of **5** is quite poor at pH values below 7, however 10 mM could be achieved in PBS buffer at pH above 7.2. As shown by the QUESP data in Fig. 2a, the contrast is near maximal at B_1 > 6 μT, with a smaller k_{sw} (1.0 kHz) than that of **4**. The peaks in the Z-spectrum and the MTR_{asym} spectrum are also sharper than those of **4** (Table S1), which is also due to a slower k_{sw}. The contrast of **5** is nearly linearly dependent with concentration over a range from 0.75 mM to 10 mM (36) (pH 7.4), with 1.2% contrast observed at a concentration of 1.5 mM (Fig. 2b).

In an attempt to increase the chemical shift further to fit the slow to intermediate detection window of CEST ($k_{sw} < \Delta\omega$) while still keeping k_{sw} slow enough for achieving efficient saturation using a B_1 suitable for the MR hardware used in our *in vivo* scans, we investigated the C2 amide analogues of anthranilic acid. Amide N-H protons tend to be shifted further than amine protons, although they also tend to exchange with water slower as well (5). As expected, **10** did not show any CEST contrast presumably because k_{sw} is too slow (Fig. 3a, Scheme 1). However, after modification of the structure to **11**, an example of a more acidic N-H proton, we observed CEST contrast with the labile proton resonating at 9.3 ppm indicating a strong hydrogen bond interaction in water. The contrast produced by **11** is relatively low (6 % at 25 mM, B_1 = 3.6 μT), because k_{sw} is relatively slow (0.3 kHz, see supplementary Figs. S2, S3 for QUESP/pH details). Further increasing the acidity through 2-(methyl-sulfonamido) benzoic acid (**12**) results in more substantial contrast at 7.3 ppm (~15 % at 25 mM, B_1 = 3.6 μT), based on adjusting the proton exchange of the IM-SHY -NH. According to our QUESP measurements, **12** displays a k_{sw} = 0.6 kHz at pH = 7.1, which is quite similar to salicylic acid (31) and barbituric acid (supplemental Fig. S5). Maximum contrast is achieved using B_1 = 6 μT or higher with ~90% of this contrast available at B_1 = 3.6 μT (Fig. 3c), which is near the maximum power we can apply using a parallel transmit

body coil on our clinical scanners. More interestingly, the contrast and k_{sw} of **11** and **12** remained almost constant between the pH values 6 – 8 (Figs. 3d, S2, S3, S4). For comparison, salicylic acid (**1**), an alternative IM-SHY agent, possesses protons with k_{sw} that decrease dramatically over this range (k_{sw} = 2.4 kHz at pH 6.5, k_{sw} = 0.4 kHz at pH 7.8). This pH independence makes **11** and **12** ideal IM-SHY probes for *in vivo* quantification purposes. As expected, a nearly linear relationship between contrast and concentration was observed for **12** (Fig. 3b), with 1% CEST contrast produced at a concentration of 1.5 mM. Although the chemical shift is not as large as **1** or **11, 12** represents the first diaCEST agent with labile N-H protons resonating at 7–8 ppm from water that produces significant contrast. This compound should be useful for multiple frequency detection and complementary to other existing diaCEST probes.

Encouraged by the result from **12**, we studied several commercially available analogues to check if the CEST contrast of this scaffold would tolerate chemical modification. As shown in Scheme 1 and Fig. 3e, similar contrast was obtained upon chemical modification of the aniline ring (**13–15**), with the CEST frequency varying from 6 ppm to 7.3 ppm. Placing a strong electron donating -NH_2 group (**15**) at the para-position to the C2-NH reduced the CEST frequency to 6.3 ppm, which is quite similar to the electronic effects we observed previously (31). Placing a –Cl at the para-position of the C2-NH (**13**) leads to faster k_{sw} (1.0 kHz), and as a result a higher CEST contrast (~20%). Substitution of a phenyl for the methyl (**16**) resulted in deshielding with the chemical shift increased to 7.8 ppm. In comparison, replacing the methyl group in 12 with a -CF3 (**17**) results in loss of CEST contrast. As this group of agents, **12–16**, generated similar contrast to **1** in phantoms, we further chose to monitor *in vivo* the contrast in kidneys after administration into the tail vein of mice of the most sensitive, **13** (Fig. 4). The contrast was monitored over time, and compared to the pre-injection images (Fig.4b), we observed a 2–3% increase in the CEST contrast 7.5 minutes after injection integrating from 7.0 – 7.6 ppm (Figs. 4b,c). The histogram in Fig. 4d indicates the pixelwise distribution of MTR_{asym} values for mouse 1 pre- and post-injection. A negative MTR_{asym} was observed as baseline for the kidneys, which is presumably due to strong relayed NOE transfer of signal loss to water (37,38). As shown in Fig.4e, for both mice the contrast reaches maximum at ~7.5 mins. post-injection

As is shown above, anthranilic acid IM-SHY probes have larger shifts for their exchangeable protons than spherical lipoCEST agents(10), and similar shifts to those found for paraCEST probes such as Yb-DO3A-oAA(39). The shifts are not nearly as large as some of the Yb, Eu, Tm or Dy complexes described previously(40–43) or the cryptophane cages used for hyperCEST(43) however because k_{sw} can be tuned as slow as 0.5 – 1 kHz through structure changes and is insensitive to pH in the physiologically relevant range, these USHY probes are well suited for detection using saturation pulses attainable on clinical scanners. A more detailed investigation of the steric and electronic factors for this scaffold is ongoing.

Conclusion

We have demonstrated that anthranilic acid provide a suitable scaffold for tunable IM-SHY diaCEST agents. Labile protons in N-aryl anthranilic acids (**4–6**) resonate at 4.8 ppm while for N-sulfonyl anthranilic acids (**12–16**) these resonate between 6 – 8 ppm and for **11** labile

protons resonate at 9.3 ppm. Anthranilic acid analogues could be used for multi-color MR imaging, with one NSAID, **5**, already administered to patients, having been identified among these analogues. The 2-sulfonamidobenzoic acid scaffold has been shown to allow chemical modification with labile protons that exchange in a non-pH dependent manner, which could be advantageous for *in vivo* quantification. Additional studies are ongoing to improve our understanding of the relationship between CEST properties and molecular structure for these and other IM-SHY diaCEST agents.

Experimental Section

Phantom Preparation and data acquisition

Compounds **1 – 12** were purchased from Sigma Aldrich (St. Louis, MO). Compounds **13–17** were purchased from Enamine Ltd (Monmouth, NJ). Samples were dissolved in 0.01 M phosphate-buffered saline (PBS) at several concentrations from 1.5 mM up to 25 mM depending on the solubility, and titrated using high concentration HCl/NaOH to various pH values ranging from 6 to 8. The solutions were placed into 1 mm glass capillaries and assembled in a holder for CEST MR imaging. They were kept at 37 °C during imaging. Phantom CEST experiments were performed on a Bruker 11.7 T vertical bore MR scanner, using a 20 mm birdcage transmit/receive coil. CEST images were acquired using a RARE (RARE factor = 8) sequence with a continuous wave (CW) saturation pulse length of 3 s and saturation field strength (B_1) from 1.2 μT to 14.4 μT. The CEST Z-spectra were acquired by incrementing the saturation frequency every 0.3 ppm from −15 to 15 ppm; TR /effective TE = 6s/17 ms with linear phase-encoding, matrix size = 64*48 and slice thickness = 1.2 mm. For determining k_{sw} using QUESP, Z-spectra were collected at B_1 = 1.2 μT, 2.4 μT, 3.6 μT, 5.4 μT, 7.2 μT, 10.8 μT and 11.4 μT.

In vivo mouse imaging

To evaluate whether the N-sulfonyl derivatives, **12–16,** could be detected after administration into live animals, we injected two mice with 60 μL of a 0.25 M solution of compound **13** and collected CEST images. Images consisting of a single axial slice containing both kidneys were collected. To improve the temporal resolution and able to correct the B_0 shift, we collected a partial z-spectrum every five minutes by incrementing Δω over ten frequencies: [±8.2 ppm, ±7.6 ppm, ±7.3 ppm, ±7 ppm, ±6.6 ppm], and an average MTR_{asym} at [±7.6 ppm, ±7.3 ppm, ±7 ppm]. The imaging sequence employed is the same as for the phantoms, with the following parameters:B_1 = 3.6 μT, T_{sat} = 3 s, TR/ effective TE = 5 s/16 ms with linear phase-encoding, matrix size 96×64.

Post-processing

CEST contrast was quantified using MTR_{asym} = (S(−Δω)–S(+Δω))/$S_0$for phantom and 1-S(+Δω)/ S(−Δω) for *in vivo* to increase the temporal resolution and reduce the motion where S(+Δω) represents water signal intensity with a saturation pulse applied at the frequency +Δω and S_0 represents the water signal without a saturation pulse. The Z-spectra were corrected pixel by pixel using a B0 map acquired using WASSR as described in detail previously (9). To indicate the kinetics of CEST contrast upon injection of the agents, we subtracted the MTR_{asym} values at each time-point with a reference MTRasym(0) at pre-

injection, i.e. ΔMTR_{asym} (t) = MTR_{asym} (t) – MTR_{asym} (0), and plotted the averaged ΔMTRasym (t) of the whole kidney as a function of minutes post-injection. The solvent to water exchange rate (k_{sw}) was calculated according to the QUEST and/or QUESP methods (34), which were considered as a simple and robust method for estimating k_{sw}, especially for the slow to intermediate exchange regime(44,45). In particular we numerically solvedthe 2-pool model Bloch equations to fit the measured MTR_{asym} values as a function of different T_{sat} or B_1 as described previously (34), with the parameters for the fittings: $R_{2w} = 0.9\ s^{-1}$, $R_{1s} = 0.71\ s^{-1}$, $R_{2s} = 39\ s^{-1}$, $T_{sat} = 3$ s. R_{1w} was allowed to float between 0.33 – 0.40 s^{-1} to obtain the best fit. The QUESP/QUEST fittings are shown in supplemental Figs. S1–S5.

Supplementary Material

Refer to Web version on PubMed Central for supplementary material.

Acknowledgments

This was supported by NIH grant number NIH R01 EB012590, R01 EB015031,U54CA151838.

References

1. Ward KM, Aletras AH, Balaban RS. A new class of contrast agents for MRI based on proton chemical exchange dependent saturation transfer (CEST). J Magn Reson. 2000; 143(1):79–87. [PubMed: 10698648]
2. Aime S, Delli Castelli D, Terreno E. Novel pH-reporter MRI contrast agents. Angewandte Chemie. 2002; 114(22):4510–4512.
3. Ward KM, Balaban RS. Determination of pH using water protons and chemical exchange dependent saturation transfer (CEST). Magn Reson Med. 2000; 44(5):799–802. [PubMed: 11064415]
4. De Leon-Rodriguez LM, Lubag AJM, Malloy CR, Martinez GV, Gillies RJ, Sherry AD. Responsive MRI Agents for Sensing Metabolism in Vivo. Accounts of chemical research. 2009; 42(7):948–957. [PubMed: 19265438]
5. McMahon MT, Gilad AA, DeLiso MA, Berman SM, Bulte JW, van Zijl PC. New "multicolor" polypeptide diamagnetic chemical exchange saturation transfer (DIACEST) contrast agents for MRI. Magn Reson Med. 2008; 60(4):803–812. [PubMed: 18816830]
6. Aime S, Carrera C, Delli Castelli D, Geninatti Crich S, Terreno E. Tunable Imaging of Cells Labeled with MRI-PARACEST Agents. Angew Chem Int Ed. 2005; 44(12):1813–1815.
7. Viswanathan S, Ratnakar SJ, Green KN, Kovacs Z, De Leon-Rodriguez LM, Sherry AD. Multi-frequency PARACEST agents based on europium(III)-DOTA-tetraamide ligands. Angewandte Chemie. 2009; 48(49):9330–9333. [PubMed: 19894248]
8. van Zijl PC, Yadav NN. Chemical exchange saturation transfer (CEST): what is in a name and what isn't? Magn Reson Med. 2011; 65(4):927–948. [PubMed: 21337419]
9. Liu G, Song X, Chan KW, McMahon MT. Nuts and bolts of chemical exchange saturation transfer MRI. NMR Biomed. 2013; 26(7):810–828. [PubMed: 23303716]
10. Castelli DD, Terreno E, Longo D, Aime S. Nanoparticle-based chemical exchange saturation transfer (CEST) agents. NMR Biomed. 2013; 26(7):839–849. [PubMed: 23784956]
11. Soesbe TC, Wu Y, Dean Sherry A. Advantages of paramagnetic chemical exchange saturation transfer (CEST) complexes having slow to intermediate water exchange properties as responsive MRI agents. NMR Biomed. 2013; 26(7):829–838. [PubMed: 23055299]
12. Chan KW, McMahon MT, Kato Y, Liu G, Bulte JW, Bhujwalla ZM, Artemov D, van Zijl PC. Natural D-glucose as a biodegradable MRI contrast agent for detecting cancer. Magn Reson Med. 2012; 68(6):1764–1773. [PubMed: 23074027]

13. Walker-Samuel S, Ramasawmy R, Torrealdea F, Rega M, Rajkumar V, Johnson SP, Richardson S, Goncalves M, Parkes HG, Arstad E, Thomas DL, Pedley RB, Lythgoe MF, Golay X. In vivo imaging of glucose uptake and metabolism in tumors. Nature medicine. 2013
14. Jin T, Autio J, Obata T, Kim S-G. Spin-locking versus chemical exchange saturation transfer MRI for investigating chemical exchange process between water and labile metabolite protons. Magnetic Resonance in Medicine. 2011; 65(5):1448–1460. [PubMed: 21500270]
15. van Zijl PC, Jones CK, Ren J, Malloy CR, Sherry AD. MRI detection of glycogen in vivo by using chemical exchange saturation transfer imaging (glycoCEST). Proc Natl Acad Sci U S A. 2007; 104(11):4359–4364. [PubMed: 17360529]
16. Haris M, Cai K, Singh A, Hariharan H, Reddy R. In vivo mapping of brain myo-inositol. Neuroimage. 2011; 54(3):2079–2085. [PubMed: 20951217]
17. Cai K, Haris M, Singh A, Kogan F, Greenberg JH, Hariharan H, Detre JA, Reddy R. Magnetic resonance imaging of glutamate. Nature Medicine. 2012; 18(2):302–306.
18. Haris M, Nanga RP, Singh A, Cai K, Kogan F, Hariharan H, Reddy R. Exchange rates of creatine kinase metabolites: feasibility of imaging creatine by chemical exchange saturation transfer MRI. NMR Biomed. 2012; 25(11):1305–1309. [PubMed: 22431193]
19. Kogan F, Haris M, Singh A, Cai K, Debrosse C, Nanga RP, Hariharan H, Reddy R. Method for high-resolution imaging of creatine in vivo using chemical exchange saturation transfer. Magn Reson Med. 2013
20. Chan KW, Liu G, Song X, Kim H, Yu T, Arifin DR, Gilad AA, Hanes J, Walczak P, van Zijl PC, Bulte JW, McMahon MT. MRI-detectable pH nanosensors incorporated into hydrogels for in vivo sensing of transplanted-cell viability. Nat Mater. 2013; 12(3):268–275. [PubMed: 23353626]
21. Liu G, Moake M, Har-el YE, Long CM, Chan KW, Cardona A, Jamil M, Walczak P, Gilad AA, Sgouros G, van Zijl PC, Bulte JW, McMahon MT. In vivo multicolor molecular MR imaging using diamagnetic chemical exchange saturation transfer liposomes. Magn Reson Med. 2012; 67(4):1106–1113. [PubMed: 22392814]
22. Saar G, Zhang B, Ling W, Regatte RR, Navon G, Jerschow A. Assessment of glycosaminoglycan concentration changes in the intervertebral disc via chemical exchange saturation transfer. NMR Biomed. 2012; 25(2):255–261. [PubMed: 22253087]
23. Ling W, Regatte RR, Navon G, Jerschow A. Assessment of glycosaminoglycan concentration in vivo by chemical exchange-dependent saturation transfer (gagCEST). Proc Natl Acad Sci U S A. 2008; 105(7):2266–2270. [PubMed: 18268341]
24. Gilad AA, McMahon MT, Walczak P, Winnard PT Jr, Raman V, van Laarhoven HW, Skoglund CM, Bulte JW, van Zijl PC. Artificial reporter gene providing MRI contrast based on proton exchange. Nature Biotechnology. 2007; 25(2):217–219.
25. Zhou J, Lal B, Wilson DA, Laterra J, van Zijl PC. Amide proton transfer (APT) contrast for imaging of brain tumors. Magn Reson Med. 2003; 50(6):1120–1126. [PubMed: 14648559]
26. Airan RD, Bar-Shir A, Liu G, Pelled G, McMahon MT, van Zijl PC, Bulte JW, Gilad AA. MRI biosensor for protein kinase A encoded by a single synthetic gene. Magn Reson Med. 2012; 68(6): 1919–1923. [PubMed: 23023588]
27. Hancu I, Dixon WT, Woods M, Vinogradov E, Sherry AD, Lenkinski RE. CEST and PARACEST MR contrast agents. Acta Radiol. 2010; 51(8):910–923. [PubMed: 20828299]
28. Bar-Shir A, Liu G, Liang Y, Yadav NN, McMahon MT, Walczak P, Nimmagadda S, Pomper MG, Tallman KA, Greenberg MM, van Zijl PC, Bulte JW, Gilad AA. Transforming thymidine into a magnetic resonance imaging probe for monitoring gene expression. Journal of the American Chemical Society. 2013; 135(4):1617–1624. [PubMed: 23289583]
29. Aime S, Calabi L, Biondi L, De Miranda M, Ghelli S, Paleari L, Rebaudengo C, Terreno E. Iopamidol: Exploring the potential use of a well-established X-ray contrast agent for MRI. Magnetic Resonance in Medicine. 2005; 53(4):830–834. [PubMed: 15799043]
30. Longo DL, Dastru W, Digilio G, Keupp J, Langereis S, Lanzardo S, Prestigio S, Steinbach O, Terreno E, Uggeri F, Aime S. Iopamidol as a responsive MRI-chemical exchange saturation transfer contrast agent for pH mapping of kidneys: In vivo studies in mice at 7 T. Magn Reson Med. 2011; 65(1):202–211. [PubMed: 20949634]

31. Yang X, Song X, Li Y, Liu G, Ray Banerjee S, Pomper MG, McMahon MT. Salicylic Acid and Analogs: Diamagnetic Chemical Exchange Satuation Transfer (diaCEST) Magnetic Resonance Imaging (MRI) Contrast Agents with Highly Shifted Exchangeable Protons. Angew Chemie Int Ed. 2013; 52(31):8116–8119.
32. Maciel GE, Savitsky GB. CARBON**-- 13 CHEMICAL SHIFTS + INTRAMOLECULAR HYDROGEN BONDING. J Phys Chem. 1964; 68(2) 437-&.
33. Mock WL, Morsch LA. Low barrier hydrogen bonds within salicylate mono-anions. Tetrahedron. 2001; 57(15):2957–2964.
34. McMahon MT, Gilad AA, Zhou J, Sun PZ, Bulte JW, van Zijl PC. Quantifying exchange rates in chemical exchange saturation transfer agents using the saturation time and saturation power dependencies of the magnetization transfer effect on the magnetic resonance imaging signal (QUEST and QUESP): Ph calibration for poly-L-lysine and a starburst dendrimer. Magn Reson Med. 2006; 55(4):836–847. [PubMed: 16506187]
35. Lovering AL, Ride JP, Bunce CM, Desmond JC, Cummings SM, White SA. Crystal structures of prostaglandin D-2 11-ketoreductase (AKR1C3) in complex with the nonsteroidal anti-inflammatory drugs flufenamic acid and indomethacin. Cancer Res. 2004; 64(5):1802–1810. [PubMed: 14996743]
36. Ali MM, Liu G, Shah T, Flask CA, Pagel MD. Using two chemical exchange saturation transfer magnetic resonance imaging contrast agents for molecular imaging studies. Acc Chem Res. 2009; 42(7):915–924. [PubMed: 19514717]
37. Jones CK, Huang A, Xu J, Edden RA, Schar M, Hua J, Oskolkov N, Zaca D, Zhou J, McMahon MT, Pillai JJ, van Zijl PC. Nuclear Overhauser enhancement (NOE) imaging in the human brain at 7T. Neuroimage. 77:114–124. [PubMed: 23567889]
38. Pekar J, Jezzard P, Roberts DA, Leigh JS Jr, Frank JA, McLaughlin AC. Perfusion imaging with compensation for asymmetric magnetization transfer effects. Magn Reson Med. 1996; 35(1):70–79. [PubMed: 8771024]
39. Liu GS, Li YG, Sheth VR, Pagel MD. Imaging In Vivo Extracellular pH with a Single Paramagnetic Chemical Exchange Saturation Transfer Magnetic Resonance Imaging Contrast Agent. Mol Imaging. 2012; 11(1):47–57. [PubMed: 22418027]
40. Terreno E, Castelli DD, Aime S. Encoding the frequency dependence in MRI contrast media: the emerging class of CEST agents. Contrast Media Mol Imaging. 2010; 5(2):78–98. [PubMed: 20419761]
41. Sherry, AD.; Woods, M. Annual Review of Biomedical Engineering. Vol. Volume 10. Palo Alto: Annual Reviews; 2008. Chemical exchange saturation transfer contrast agents for magnetic resonance imaging. Annual Review of Biomedical Engineering; p. 391-411.
42. Chauvin T, Durand P, Bernier M, Meudal H, Doan B-T, Noury F, Badet B, Beloeil J-C, Tóth É. Detection of Enzymatic Activity by PARACEST MRI: A General Approach to Target a Large Variety of Enzymes. Angewandte Chemie International Edition. 2008; 47(23):4370–4372.
43. Schroder L, Lowery TJ, Hilty C, Wemmer DE, Pines A. Molecular imaging using a targeted magnetic resonance hyperpolarized biosensor. Science. 2006; 314(5798):446–449. [PubMed: 17053143]
44. Randtke EA, Chen LQ, Corrales LR, Pagel MD. The Hanes-Woolf linear QUESP method improves the measurements of fast chemical exchange rates with CEST MRI. Magn Reson Med.
45. Sun PZ. Simplified quantification of labile proton concentration-weighted chemical exchange rate (k(ws)) with RF saturation time dependent ratiometric analysis (QUESTRA): normalization of relaxation and RF irradiation spillover effects for improved quantitative chemical exchange saturation transfer (CEST) MRI. Magn Reson Med. 67(4):936–942. [PubMed: 21842497]

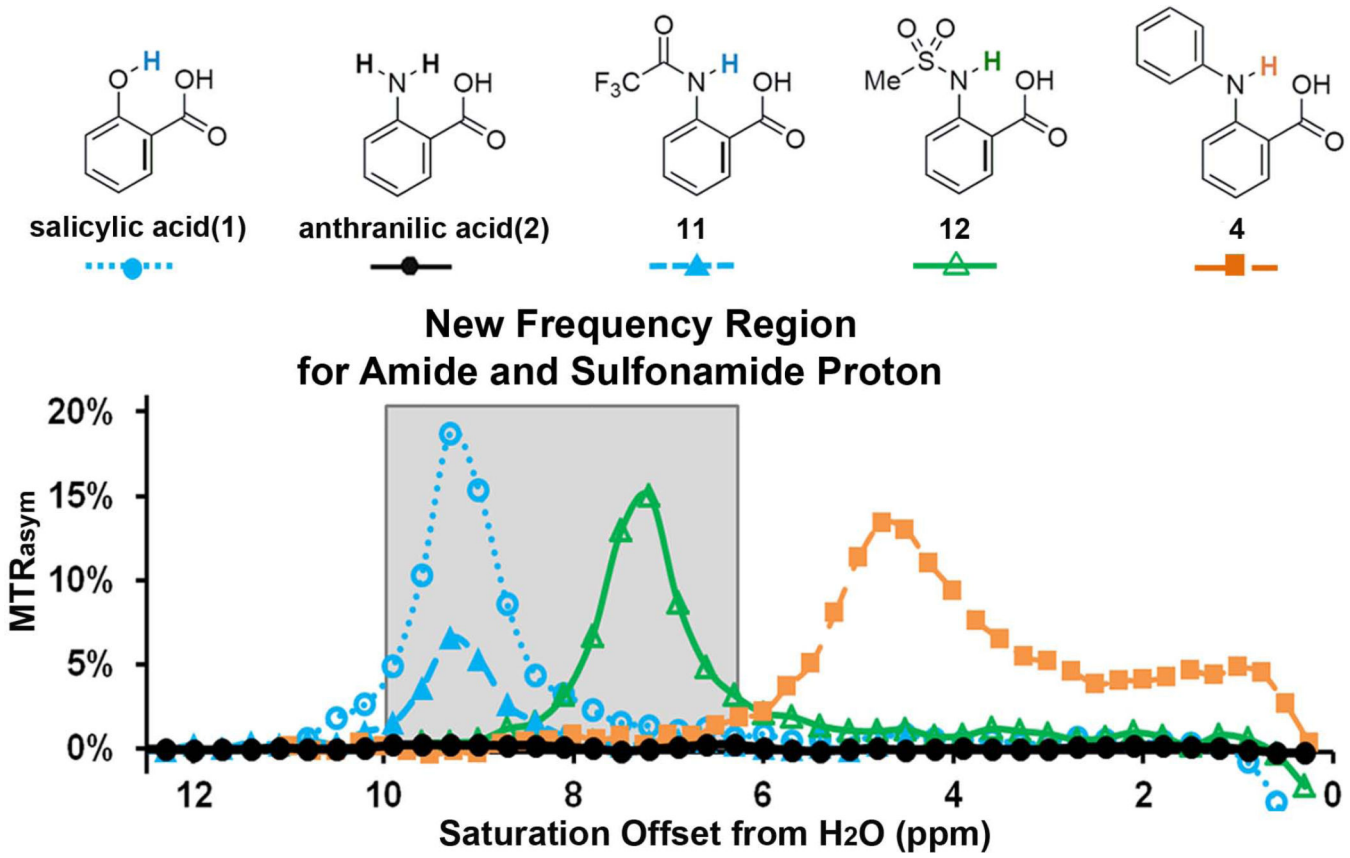

Figure 1.

CEST contrast curves for representative salicylic acid (**1**) and anthranilic acid derivatives (**2, 4, 11** and **12**) at concentrations of 25 mM (pH 7.1–7.4) using B_1 = 3.6 μT, t_{sat} = 3 s. The gray box indicates this group of agents includes a new frequency region for amide and sulfonamide protons.

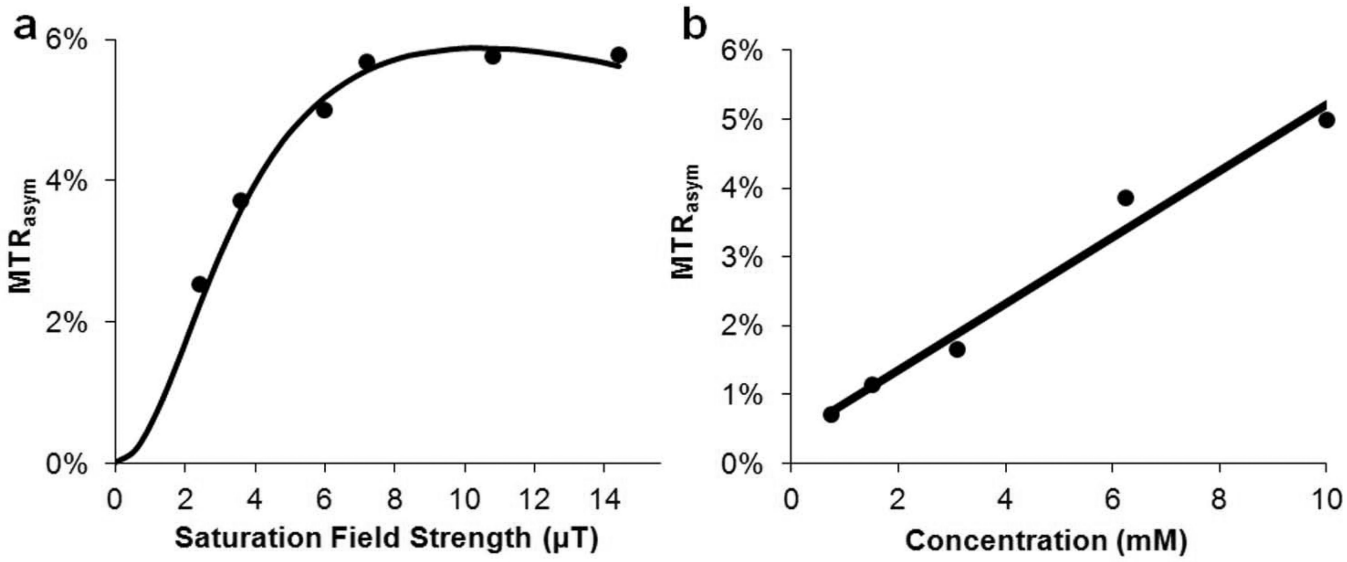

Figure 2.

CEST properties of **5**. a) QUESP data at 10 mM at pH = 7.4, with k_{sw} = 1.0 kHz where the data are shown as points and the solid line representing the best fit after numerically solving the 2-pool Bloch equations; b) CEST contrast at 4.8 ppm as a function of concentration using B_1 = 3.6 μT. (Solid line: linear fitting)

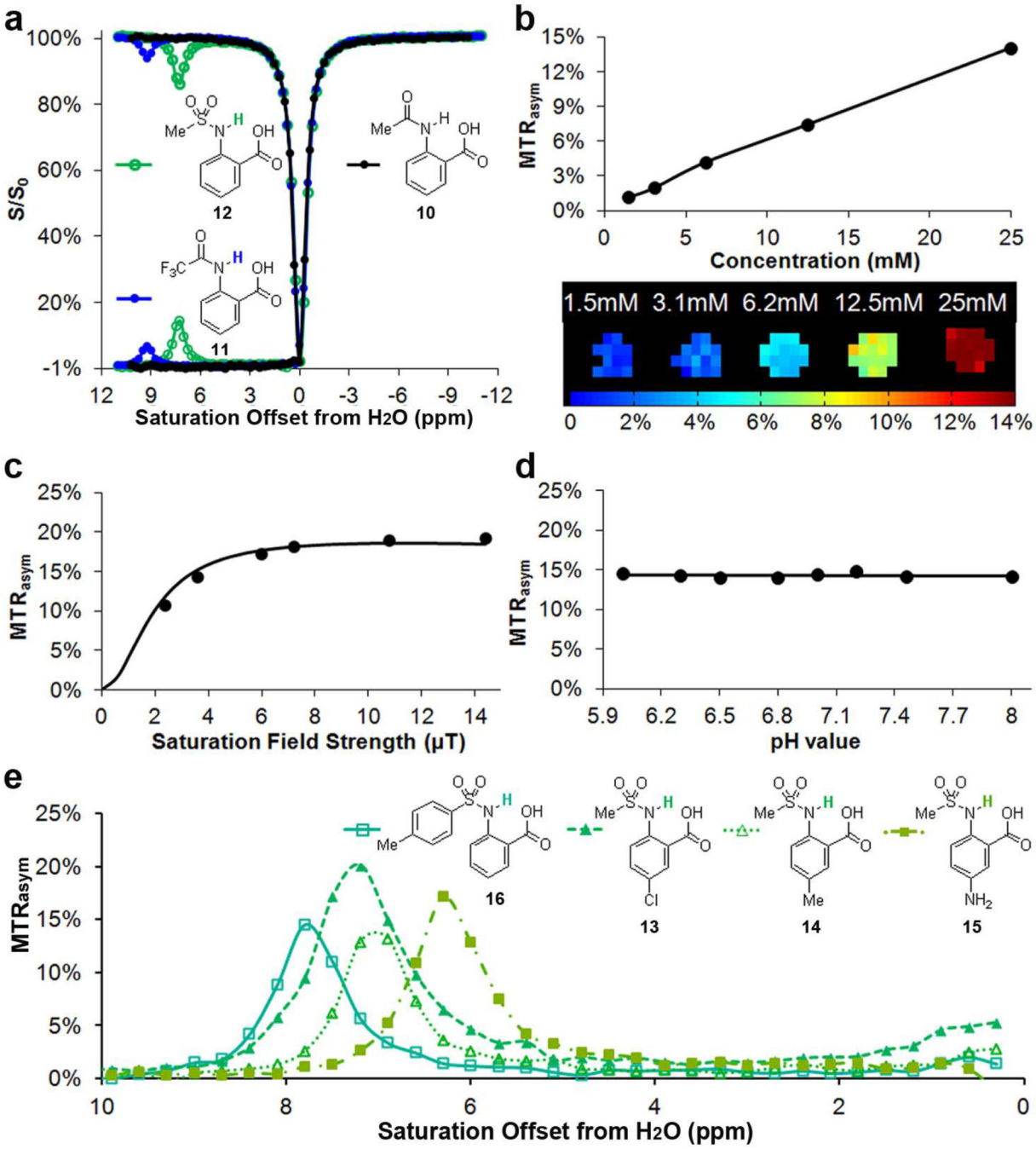

Figure 3.

CEST properties of **10 – 16**. a) Z-spectra and MTR_{asym} for **10 – 12** at 25 mM, pH = 7.2, t_{sat} = 3 s and B_1 = 3.6 μT; b) CEST contrast of **12** at 7.5 ppm as a function of concentration, using B_1 = 3.6 μT; c) QUESP data of **12** at 25 mM, pH = 7.1, with k_{sw} =0.6 kHz; d) pH dependence of % contrast for **12**; e) Analogues of **12** with different CEST peak frequencies from 6 – 8 ppm.

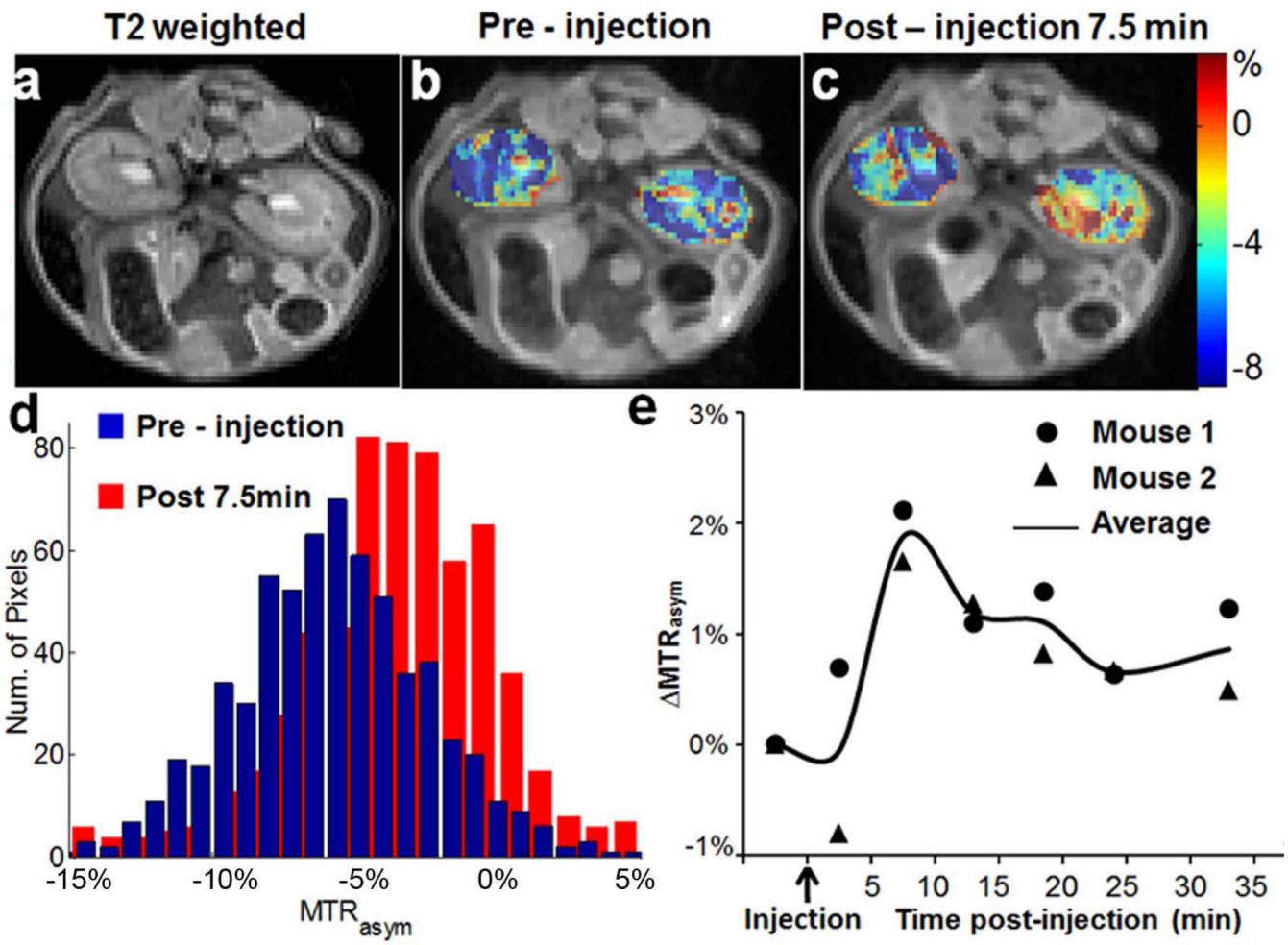

Figure 4.

In vivo contrast for **13**. a) T2w image; b) overlay MTR_{asym} map pre-injection for mouse 1; c) overlay MTR_{asym} map at 10 min post-injection for mouse 1; d) histogram displaying the distribution of MTR_{asym} for Mouse 1 pre- and post-injection (Figs.4c,d). e) dynamic time course of ΔMTR_{asym} based on ROIs enclosing both left and right kidneys for the two mice using ω_1= 3.6 μT (circle: Mouse 1, triangle: Mouse 2, solid line, average value of Mouse 1 and Mouse 2).

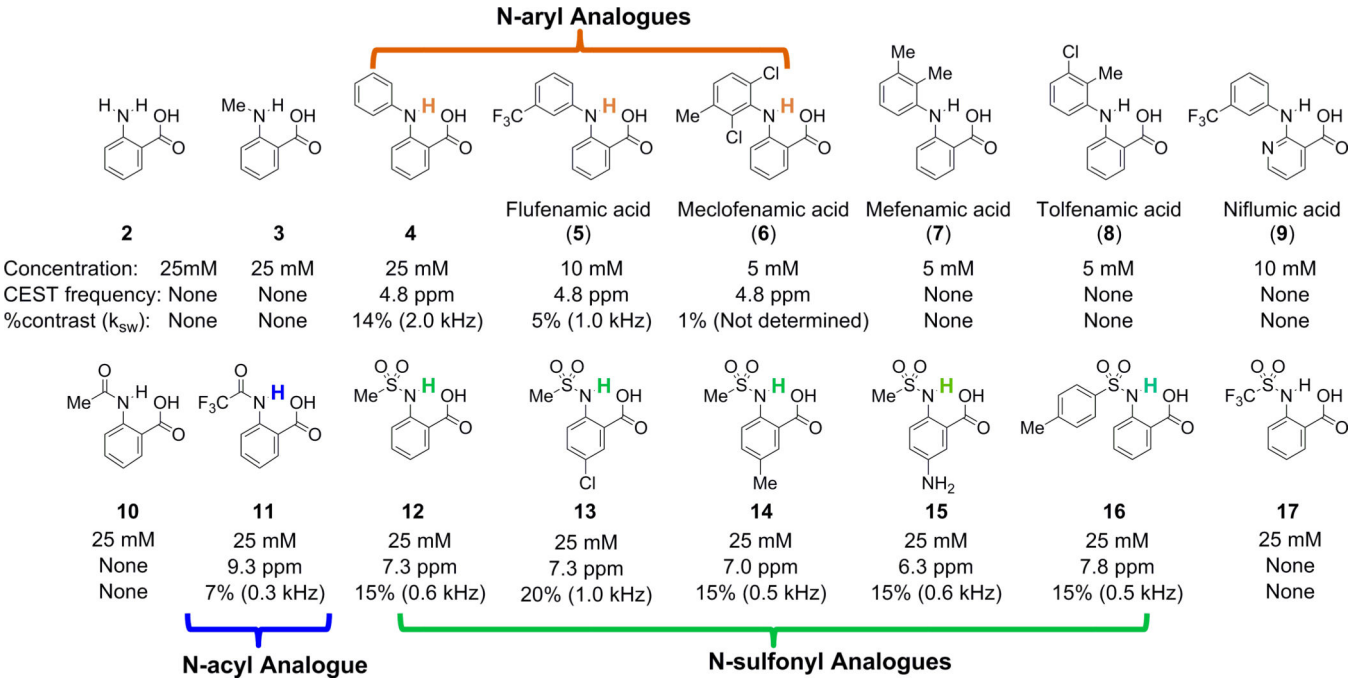

Scheme 1.

CEST frequency [ppm], contrast [%] and k_{sw}, [kHz] of anthranilic acid and its analogues. Experimental conditions: pH 7.1 –7.5, using t_{sat}=3 s, B_1=3.6 μT. For Z-spectra, see Tables S1 and S2. All the MR experiments were performed at 37°C.